Computers and Concrete, *Vol. 20, No. 2 (2017) 119-127*
DOI: https://doi.org/10.12989/cac.2017.20.2.119

Time-dependent buckling analysis of SiO_2 nanoparticles reinforced concrete columns exposed to fire

M. Rabani Bidgoli* and M. Saeidifar

Department of Civil Engineering, Jasb Branch, Islamic Azad University, Jasb, Iran

(Received February 25, 2017, Revised March 24, 2017, Accepted March 30, 2017)

Abstract. Time-dependent buckling of embedded straight concrete columns armed with Silicon dioxide(SiO_2) nano-particles exposed to fire is investigated in the present study for the fire time. The column is simulated mathematically with Timoshenko beam model. The governing mass conservation equations to describe heat and moisture transport in concrete containing free water, water vapor, and dry air in conjunction with the conversion of energy are considered. The characteristics of the equivalent composite are determined using Mori-Tanaka approach. The foundation around the column is simulated with spring and shear layer. Employing nonlinear strains-displacements, energy methods and Hamilton's principal, the governing equations are derived. Differential quadrature method (DQM) is used in order to obtain the critical buckling load and critical buckling time of structure. The influences of volume percent of SiO_2nano-particles, geometrical parameters, elastic foundation and concrete porosity are investigated on the time-dependent buckling behaviours of structure. Numerical results indicate that reinforcing the concrete column with SiO_2nano-particles, the structure becomes stiffer and the critical buckling load and time increase.

Keywords: concrete column; SiO_2nano-particles; fire; DQM; buckling

1. Introduction

Concrete is a newer construction material compared to steel and stone. Use of concrete in constructions and buildings might have begun less than a century ago. In the past few decades, many researchers have used wide range of supplementary materials like nano particles. Carbon nanotubes, Silicon dioxide (SiO_2), Nano-Clay, Aluminium oxide (AL_2O_3) and Titanium dioxide (TiO_2) are some of the naturally occurring nano particles. The use of additional cementitious materials due to economic, technical and environmental considerations has become very common in modern concrete construction.

Mechanical analysis of concrete column has been investigated by many researchers. Tan and Yao (2003) developed a simple and rational method to predict the fire resistance of reinforced concrete columns subjected to four-face heating. Fire tests and calculation methods for circular concrete columns were presented by Franssen and Dotreppe (2003). A numerical model, in the form of a computer program, for tracing the behaviour of high performance concrete (HPC) columns exposed to fire was presented by Kodur *et al.* (2004). Bratina *et al.* (2005) used a two-step finite element formulation for the thermo-mechanical non-linear analysis of the behaviour of the reinforced concrete columns in fire. The importance of capillary pressure and adsorbed water in the behaviour of heat and moisture transport in concrete exposed to high temperatures was explored by Davie *et al.* (2006) incorporating their behaviour explicitly into a computational model. A nonlinear structural analysis of cross-sections of three-dimensional reinforced concrete frames exposed to fire was studied by Capua and Mari (2007). A two-step formulation, consisting of separate thermal and mechanical analyses, was presented by Bratina and Saje (2007) for the thermo-mechanical analysis of reinforced concrete planar frames subject to fire conditions. Buckling of restrained steel columns due to fire conditions was investigated by Hozjan *et al.* (2008). Rodrigues *et al.* (2010) presented the results of a research program on the behaviour of fiber reinforced concrete columns in fire. Several fire resistance tests on fiber reinforced concrete columns with restrained thermal elongation were carried out. Buckling of axially restrained steel columns in fire was presented by Shepherd and Burgess (2011). Fire analysis of steel-concrete composite eam with interlayer slip was developed by Hozjan *et al.* (2011). A numerical technique was proposed by Bacinskas *et al.* (2012) for the long-term deformation analysis of reinforced concrete members subjected to a bending moment. Wang *et al.* (2016) presented the experimental results of bond strength between the embedded steel and concrete in steel reinforced concrete (SRC) columns after fire exposure. Bajc *et al.* (2015) derived a new semi-analytical procedure for the determination of buckling of the reinforced concrete column exposed to fire. The nonlinear buckling of straight concrete columns armed with single-walled carbon nanotubes (SWCNTs) resting on foundation was investigated by Safari Bilouei *et al.* (2016). The nonlinear buckling of straight concrete columns armed with single-walled carbon nanotubes (SWCNTs) resting on foundation was investigated by Jafarian Arani and Kolahchi (2016). The nonlinear buckling of an embedded straight concrete columns reinforced with silicon dioxide (SiO_2)

*Corresponding author, Assistant Professor
E-mail: m.rabanibidgoli@gmail.com

ISSN: 1598-8198 (Print), 1598-818X (Online)

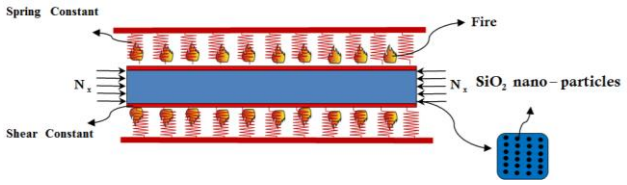

Fig. 1 Geometry of the SiO_2nano-particles-reinforced concrete column exposed to fire

nanoparticles was investigated by Zamanian *et al.* (2016).

It can be observed from literature that the theoretical researches on time-dependent buckling of concrete columns armed with SiO_2nano-particles exposed to fire are rare. The main goal of the present paper is to present a mathematical model for concrete columns exposed to fire and discuss about the nanotechnology effects. For this ends, the concrete column is modelled with Timoshenko beam model. The heat and mass transfer is described considering the transfer of free water, water vapour and dry air caused by pressure and concentration gradients and the conversion of energy. The foundation is simulated with spring and shear constants. Applying energy method and Hamilton's principal, the governing equations are derived. DQM is used for obtaining the critical buckling load and time of structure. The effects of different parameters such as volume percent of SiO_2nano-particles, geometrical parameters, elastic foundation, and concrete porosity on the time-dependent buckling of concrete columns are discussed.

2. Mathematical modelling

Fig. 1 shows a SiO_2nano-particles-reinforced concrete column exposed to fire with length L and thickness h embedded in foundation. The surrounding foundation is described by the spring constant k_w and shear layer k_g.

2.1 Timoshenko beam model

The concrete column is modelled with Timoshenko beam. The displacements of an arbitrary point in the beam are (Brush and Almroth 1975)

$$\begin{aligned} u_1(x,z) &= U(x) + z\psi(x), \\ u_2(x,z) &= 0, \\ u_3(x,z) &= W(x) \end{aligned} \tag{1}$$

Where $U(x, t)$ and $W(x, t)$ are displacement components in the mid-plane, ψ is the rotation of beam cross-section. The von Karman type nonlinear strain-displacement relations are given by

$$\varepsilon_{xx} = \frac{\partial U}{\partial x} + z\frac{\partial \psi}{\partial x} + \frac{1}{2}\left(\frac{\partial W}{\partial x}\right)^2, \tag{2}$$

$$\gamma_{xz} = \frac{\partial W}{\partial x} + \psi. \tag{3}$$

In addition, the stress-strain relations can be written as

$$\sigma_{xx} = C_{11}\left(\varepsilon_x - \alpha_x T\right), \tag{4}$$

$$\sigma_{xz} = C_{55}\left[\frac{\partial W}{\partial x} + \psi\right], \tag{5}$$

where C_{11} and C_{22} are elastic constants.

2.2 Energy method

2.2.1 Potential energy

The potential energy of the structure can be expressed as

$$U = \frac{1}{2}\int_0^L \int_A (\sigma_{xx}\varepsilon_{xx} + 2\sigma_{xz}\varepsilon_{xz})\, dA dx \tag{6}$$

Submitting Eqs. (2) and (3) into Eq. (6) gives

$$U = \frac{1}{2}\int_0^L \int_A \left\{ \begin{array}{l} \sigma_x \left[\begin{array}{l} \dfrac{\partial U}{\partial x} + z\dfrac{\partial \psi}{\partial x} + \dfrac{1}{2}\left(\dfrac{\partial W}{\partial x}\right)^2 \\ -\alpha_x T \end{array} \right] \\ +\sigma_{xz}\left[\dfrac{\partial W}{\partial x} + \psi\right] \end{array} \right\} dA\, dx \tag{7}$$

where the resultant force (N_x, Q_x)and bending moment M_x are defined as

$$N_x = \int_A \sigma_{xx}\, dA, \tag{8}$$

$$M_x = \int_A \sigma_{xx} z\, dA, \tag{9}$$

$$Q_x = K_s \int_A \sigma_{xz}\, dA, \tag{10}$$

where K_s is shear correction factor.

2.2.2 Kinetic energy

The kinetic energy of the structure can be expressed as

$$K_{tube} = \frac{1}{2}\rho \int_0^l \int_A \left[\left(\frac{\partial U}{\partial t} + z\frac{\partial \psi}{\partial t}\right)^2 + \left(\frac{\partial W}{\partial t}\right)^2\right] dA dx \tag{11}$$

where ρ is the density of structure.

2.2.3 External work

The force induced by the foundation is denoted by (Ghorbanpour Arani *et al.* 2015)

$$F_{ElasticMedium} = k_w W - k_g \nabla^2 W \tag{12}$$

The governing mass conservation equations to describe heat and moisture transport in concrete containing free water, water vapor, and dry air can be defined as follows (Colin *et al.* 2006)

$$\frac{\partial\left(\varepsilon_G \rho_V\right)}{\partial t} = -\nabla.\mathrm{J}_V + \dot{E}_{EW}, \tag{13}$$

$$\frac{\partial\left(\varepsilon_G\hat{\rho}_A\right)}{\partial t}=-\nabla.\mathbf{J}_A, \tag{14}$$

$$\frac{\partial\left(\varepsilon_{FW}\rho_L\right)}{\partial t}=-\nabla.\mathrm{J}_{FW}-\dot{E}_{FW}+\frac{\partial\left(\varepsilon_D\rho_L\right)}{\partial t}, \tag{15}$$

where ε_i is the volume fraction of a phase i, ρ_i is the density of a phase i, $\hat{\rho}_i$ is the mass of a phasei per unit volume of gaseous material, J_i is the mass flux of a phase, $\dot{E}_{FW}$ is the rate of evaporation of free water (including desorption), t is time, and i=*FE, V, A, D* are respectively free water, water vapor, dry air, and dehydrated water phases. The energy conservation for the system can be defined as

$$\begin{aligned}\rho C\frac{\partial T}{\partial t}&=-\nabla.\left(-k\nabla T\right)-\left(\rho C\mathrm{v}\right)\nabla T-\\&\lambda_E\dot{E}_{FW}-\lambda_D\frac{\partial\left(\varepsilon_D\rho_L\right)}{\partial t},\end{aligned} \tag{16}$$

where ρC is the heat capacity of concrete, k is the thermal conductivity of concrete, $\rho C\mathrm{v}$ relates to the energy transferred by fluid flow, λ_E is the specific heat of evaporation (or of desorption when appropriate), λ_D is the specific heat of dehydration, and T is the absolute temperature. Substituting $\dot{E}_{FW}$ from Eq. (13) into Eqs. (14)-(16) yields

$$\frac{\partial\left(\varepsilon_G\hat{\rho}_A\right)}{\partial t}=-\nabla.\mathbf{J}_A, \tag{17}$$

$$\begin{aligned}&\frac{\partial\left(\varepsilon_G\hat{\rho}_V\right)}{\partial t}+\frac{\partial\left(\varepsilon_{FW}\rho_L\right)}{\partial t}-\frac{\partial\left(\varepsilon_D\rho_L\right)}{\partial t}=\\&-\nabla.\left(\mathrm{J}_{FW}+\mathrm{J}_V\right),\end{aligned} \tag{18}$$

$$\begin{aligned}&\rho C\frac{\partial T}{\partial t}-\lambda_E\frac{\partial\left(\varepsilon_{FW}\rho_L\right)}{\partial t}+\left(\lambda_E+\lambda_D\right)\frac{\partial\left(\varepsilon_D\rho_L\right)}{\partial t}=\\&\nabla.\left(k\nabla T\right)+\lambda_E\nabla.\mathrm{J}_{FW}-\left(\rho C\mathrm{v}\right).\nabla T,\end{aligned} \tag{19}$$

Based on Fick's laws, the mass fluxes of dry air, water vapor, and free water can be expressed in terms of pressure and concentration gradients as

$$\mathrm{J}_A=\varepsilon_G\hat{\rho}_A\mathrm{v}_G-\varepsilon_G\hat{\rho}_G D_{AV}\nabla\left(\frac{\hat{\rho}_A}{\hat{\rho}_G}\right), \tag{20}$$

$$\mathbf{J}_V=\varepsilon_G\hat{\rho}_V\mathbf{v}_G-\varepsilon_G\hat{\rho}_G D_{VA}\nabla\left(\frac{\hat{\rho}_V}{\hat{\rho}_G}\right), \tag{21}$$

$$\mathbf{J}_{FW}=\varepsilon_{FW}\rho_L\mathbf{v}_L, \tag{22}$$

where D_{AV} and D_{VA} are respectively the diffusion coefficients of dry air in water vapor and water vapor in dry air within the porous concrete (which are subsequently assumed to be equal (Colin *et al.* 2006)), and v_G and v_L are the velocities of the gas and liquid water phases resulting from pressure-driven flow as given by Darcy's law.

$$\mathbf{v}_G=-\frac{\overline{K}K_G}{\mu_G}\nabla P_G, \tag{23}$$

$$\mathbf{v}_L=-\frac{\overline{K}K_L}{\mu_L}\nabla P_L, \tag{24}$$

where $\overline{K}$ is the intrinsic permeability of the dry concrete, K_G and K_L are the relative permeability of the gas and liquid phases, μ_G and μ_L are their dynamic viscosities, and P_G and P_L are the corresponding pressures which can be assumed equal to each other's (Capua and Mari 2007). After extensive algebraic manipulation, the system of governing differential equations can be written in the form (Colin *et al.* 2006).

$$\begin{aligned}&C_{TT}\frac{\partial T}{\partial t}+C_{TP}\frac{\partial P_G}{\partial t}+C_{TV}\frac{\partial\hat{\rho}_V}{\partial t}=\\&\nabla.\left(K_{TT}\nabla T+K_{TP}\nabla P_G+K_{TV}\nabla\hat{\rho}_V\right),\end{aligned} \tag{25}$$

$$\begin{aligned}&C_{AT}\frac{\partial T}{\partial t}+C_{AP}\frac{\partial P_G}{\partial t}+C_{AV}\frac{\partial\hat{\rho}_V}{\partial t}=\\&\nabla.\left(K_{AT}\nabla T+K_{AP}\nabla P_G+K_{AV}\nabla\hat{\rho}_V\right),\end{aligned} \tag{26}$$

$$\begin{aligned}&C_{MT}\frac{\partial T}{\partial t}+C_{MP}\frac{\partial P_G}{\partial t}+C_{MV}\frac{\partial\hat{\rho}_V}{\partial t}=\\&\nabla.\left(K_{MT}\nabla T+K_{MP}\nabla P_G+K_{MV}\nabla\hat{\rho}_V\right),\end{aligned} \tag{27}$$

where C_{ij} and K_{ij} are defined in Appendix A.

However, the work done by the elastic medium and fire can be written as

$$W=\int_0^L\left(\underbrace{F_{Elasticmedium}+LP_G}_{q}\right)Wdx. \tag{28}$$

2.3 Hamilton's principle

The governing equations of structure can be derived from the Hamilton's principle as

$$\int_{t_0}^{t_1}\left[\delta U-\left(\delta K+\delta W\right)\right]=0 \tag{29}$$

Using above relation, the governing equations may be derived as

$$C_{11}\frac{\partial^2 U}{\partial x^2}+C_{11}\frac{\partial^2 W}{\partial x^2}\frac{\partial W}{\partial x}=\rho h\frac{\partial^2 U}{\partial t^2}, \tag{30}$$

$$\begin{aligned}&C_{55}A\left[\frac{\partial^2 W}{\partial x^2}+\frac{\partial \psi}{\partial x}\right]+N_x^M\frac{\partial^2 W}{\partial x^2}-C_{11}A\alpha_x\frac{\partial T}{\partial x}\frac{\partial W}{\partial x}\\&-C_{11}A\alpha_x T\frac{\partial^2 W}{\partial x^2}-LP_G\\&-K_w W+G_p\nabla^2 W=\rho h\frac{\partial^2 W}{\partial t^2},\end{aligned} \tag{31}$$

$$C_{11}I\frac{\partial^2 \psi}{\partial x^2}+K_s C_{55}A\left[\frac{\partial W}{\partial x}+\psi\right]=\frac{\rho h^3}{12}\frac{\partial^2 \psi}{\partial t^2}. \tag{32}$$

where N_x^M is the axial mechanical load applied to the concrete column.

The mechanical boundary conditions at both ends of column are Clamped-Clamped (CC). Hence

$$x=0,L\Rightarrow U=W=\psi=\frac{\partial W}{\partial x}=0, \tag{33}$$

Based on energy conservation equation, the temperature gradient across the boundary can be expressed as

$$x=0,L\Rightarrow\frac{\partial T}{\partial x}=\frac{h_{qr}}{k}(T_\infty-T), \tag{34}$$

For the gas pressure boundary condition, it may be noted that the gas pressure on the boundary will always be equal to the atmospheric pressure and so the gas pressure gradient across the boundary will always be zero

$$x=0,L\Rightarrow\frac{\partial P_G}{\partial x}=0, \tag{35}$$

Based on mass conservation, the mass conservation of water vapor on the boundary can be written as

$$\begin{aligned}&x=0,L\Rightarrow\frac{\partial \hat{\rho}_V}{\partial x}=\\&-\frac{K_{VT}}{K_{VV}}\frac{h_{qr}}{k}(T_\infty-T)+\frac{\beta}{K_{VV}}(\hat{\rho}_{V\infty}-\hat{\rho}_V),\end{aligned} \tag{36}$$

In addition, the initial boundary conditions can be written as

$$\begin{aligned}&t=0\Rightarrow\\&U=W=\psi=0,T=T_\infty,P_G=0,\hat{\rho}_V=\hat{\rho}_{V\infty}.\end{aligned} \tag{37}$$

Since the boundary conditions are non-classical, assuming $T-T_\infty=\theta$ and $\hat{\rho}_V-\hat{\rho}_{V\infty}=\bar{\rho}_V$ and with respect to applied beam theory and $T=T(x,t)$ yields

$$C_{11}\frac{\partial^2 U}{\partial x^2}+C_{11}\frac{\partial^2 W}{\partial x^2}\frac{\partial W}{\partial x}=\rho h\frac{\partial^2 U}{\partial t^2}, \tag{38}$$

$$\begin{aligned}&C_{55}A\left[\frac{\partial^2 W}{\partial x^2}+\frac{\partial \psi}{\partial x}\right]+N_x^M\frac{\partial^2 W}{\partial x^2}\\&-C_{11}A\alpha_x\frac{\partial \theta}{\partial x}\frac{\partial W}{\partial x}\\&-C_{11}A\alpha_x T\frac{\partial^2 W}{\partial x^2}-LP_G-K_w W+G_p\nabla^2 W\\&=\rho h\frac{\partial^2 W}{\partial t^2},\end{aligned} \tag{39}$$

$$C_{11}I\frac{\partial^2 \psi}{\partial x^2}+K_s C_{55}A\left[\frac{\partial W}{\partial x}+\psi\right]=\frac{\rho h^3}{12}\frac{\partial^2 \psi}{\partial t^2}, \tag{40}$$

$$\begin{aligned}&C_{TT}\frac{\partial T}{\partial t}\theta+C_{TP}\frac{\partial P_G}{\partial t}+C_{TV}\frac{\partial \bar{\rho}_V}{\partial t}-K_{TT}\frac{\partial^2 \theta}{\partial x^2}\\&+K_{TP}\frac{\partial^2 P_G}{\partial x^2}+K_{TV}\frac{\partial^2 \bar{\rho}_V}{\partial x^2}=0,\end{aligned} \tag{41}$$

$$\begin{aligned}&C_{AT}\theta+C_{AP}\frac{\partial P_G}{\partial t}+C_{AV}\frac{\partial \bar{\rho}_V}{\partial t}-K_{AT}\frac{\partial^2 T}{\partial x^2}\theta\\&+K_{AP}\frac{\partial^2 P_G}{\partial x^2}+K_{AV}\frac{\partial^2 \bar{\rho}_V}{\partial x^2}=0,\end{aligned} \tag{42}$$

$$\begin{aligned}&C_{MT}\frac{\partial T}{\partial t}\theta+C_{MP}\frac{\partial P_G}{\partial t}+C_{MV}\frac{\partial \bar{\rho}_V}{\partial t}\\&-K_{MT}\frac{\partial^2 T}{\partial x^2}\theta+K_{MP}\frac{\partial^2 P_G}{\partial x^2}+K_{MV}\frac{\partial^2 \bar{\rho}_V}{\partial x^2}=0.\end{aligned} \tag{43}$$

and the associated boundary conditions are

$$x=0,L\Rightarrow U=W=\psi=0, \tag{44}$$

$$x=0,L\Rightarrow\frac{\partial \theta}{\partial x}=\frac{-h_{qr}\theta}{k}, \tag{45}$$

$$x=0,L\Rightarrow\frac{\partial P_G}{\partial x}=0, \tag{46}$$

$$x=0,L\Rightarrow\frac{\partial \bar{\rho}_V}{\partial x}=\frac{K_{VT}}{K_{VV}}\frac{h_{qr}\theta}{k}-\frac{\beta\bar{\rho}_V}{K_{VV}}, \tag{47}$$

$$\begin{aligned}&t=0\Rightarrow U=W=\psi=0,\theta=0,\\&P_G=0,\bar{\rho}_V=0.\end{aligned} \tag{48}$$

3. Mori-Tanaka rule

In this section, the effective modulus of the concrete reinforced by SiO_2nano-particles is developed. The SiO_2nano-particles are assumed with the dispersion of uniform in the polymer.The matrix is assumed to be elastic and isotropic, with the Young's modulus E_m and the Poisson's ratio υ_m. The constitutive relations for the composite are (Mori and Tanaka 1973)

$$\begin{Bmatrix}\sigma_{xx}\\ \sigma_{yy}\\ \sigma_{zz}\\ \sigma_{yz}\\ \sigma_{xz}\\ \sigma_{xy}\end{Bmatrix}=\begin{bmatrix}\underset{C_{11}}{k+m} & \underset{C_{12}}{l} & \underset{C_{13}}{k-m} & 0 & 0 & 0\\ \underset{C_{21}}{l} & \underset{C_{22}}{n} & \underset{C_{23}}{l} & 0 & 0 & 0\\ \underset{C_{31}}{k-m} & \underset{C_{32}}{l} & \underset{C_{33}}{k+m} & 0 & 0 & 0\\ 0 & 0 & 0 & \underset{C_{44}}{p} & 0 & 0\\ 0 & 0 & 0 & 0 & \underset{C_{55}}{m} & 0\\ 0 & 0 & 0 & 0 & 0 & \underset{C_{66}}{p}\end{bmatrix}\begin{Bmatrix}\varepsilon_{xx}\\ \varepsilon_{yy}\\ \varepsilon_{zz}\\ \gamma_{yz}\\ \gamma_{xz}\\ \gamma_{xy}\end{Bmatrix}, \quad (49)$$

where σ_{ij}, ε_{ij}, γ_{ij}, k, m, n, l, p are the stress components, the strain components and the stiffness coefficients respectively. According to the Mori-Tanaka method the stiffness coefficients are given by (Mori and Tanaka 1973)

$$\begin{aligned}
k&=\frac{E_m\{E_m c_m+2k_r(1+\nu_m)[1+c_r(1-2\nu_m)]\}}{2(1+\nu_m)[E_m(1+c_r-2\nu_m)+2c_m k_r(1-\nu_m-2\nu_m^2)]}\\
l&=\frac{E_m\{c_m\nu_m[E_m+2k_r(1+\nu_m)]+2c_r l_r(1-\nu_m^2)]\}}{(1+\nu_m)[E_m(1+c_r-2\nu_m)+2c_m k_r(1-\nu_m-2\nu_m^2)]}\\
n&=\frac{E_m^2 c_m(1+c_r-c_m\nu_m)+2c_m c_r(k_r n_r-l_r^2)(1+\nu_m)^2(1-2\nu_m)}{(1+\nu_m)[E_m(1+c_r-2\nu_m)+2c_m k_r(1-\nu_m-2\nu_m^2)]}\\
&\quad+\frac{E_m[2c_m^2 k_r(1-\nu_m)+c_r n_r(1+c_r-2\nu_m)-4c_m l_r\nu_m]}{E_m(1+c_r-2\nu_m)+2c_m k_r(1-\nu_m-2\nu_m^2)}\\
p&=\frac{E_m[E_m c_m+2p_r(1+\nu_m)(1+c_r)]}{2(1+\nu_m)[E_m(1+c_r)+2c_m p_r(1+\nu_m)]}\\
m&=\frac{E_m[E_m c_m+2m_r(1+\nu_m)(3+c_r-4\nu_m)]}{2(1+\nu_m)\{E_m[c_m+4c_r(1-\nu_m)]+2c_m m_r(3-\nu_m-4\nu_m^2)\}}
\end{aligned} \quad (50)$$

where C_m and C_r are the volume fractions of the concrete and the SiO_2nano-particles, respectively and k_r ,l_r, n_r, p_r, m_r are the Hills elastic modulus for the SiO_2nano-particles (Mori and Tanaka 1973).

4. DQM

The main idea of the DQM is that the derivative of a function at a sample point can be approximated as a weighted linear summation of the function value at all of the sample points in the domain. The functions f={U, W, ψ, T, P_G, $\widehat{\rho}_V$ } and their kth derivatives with respect to x and t can be approximated as (Kolahchi *et al.* 2015, 2016).

$$\frac{d^n f_x(x_i,t_j)}{dx^n}=\sum_{k=1}^{N_x}A_{ik}^{(n)}f(x_k,t_j) \quad n=1,...,N_x-1. \quad (51)$$

$$\frac{d^m f_y(x_i,t_j)}{dt^m}=\sum_{l=1}^{N_t}B_{jl}^{(m)}f(x_i,t_l) \quad m=1,...,N_t-1. \quad (52)$$

$$\frac{d^{n+m} f_{xy}(x_i,t_j)}{dx^n dt^m}=\sum_{k=1}^{N_x}\sum_{l=1}^{N_t}A_{ik}^{(n)}B_{jl}^{(m)}f(x_k,t_l). \quad (53)$$

where N_x and N_t are the total number of nodes distributed along the x and t, respectively which can be expressed as

$$X_i=\frac{L}{2}\left[1-\cos\left(\frac{i-1}{N_x-1}\right)\pi\right] \qquad i=1,...,N. \quad (54)$$

$$T_i=\frac{i}{n}, \quad i=1,2,3,...,t, \quad (55)$$

In addition, A_{ij} is the weighting coefficients for x direction which for the first derivative can be written as

$$A_{ij}^{(1)}=\begin{cases}\dfrac{M(x_i)}{(x_i-x_j)M(x_j)} & for \quad i\neq j, \quad i,j=1,2,...,N_x\\ -\sum\limits_{\substack{j=1\\ i\neq j}}^{N_x}A_{ij}^{(1)} & for \quad i=j, \quad i,j=1,2,...,N_x\end{cases} \quad (56)$$

Where

$$M(x_i)=\prod_{\substack{j=1\\ j\neq i}}^{N_x}(x_i-x_j) \quad (57)$$

The weighting coefficients for $t(B_{ij})$ considering Teoplitz matrix can be expressed as

$$\begin{cases}a_{11}=0,\\ a_{i,1}=(-1)^{i-1}\cot\left(\frac{\pi(i-1)}{n}\right),\\ a_{1,j}=(-1)^{n-j+1}\cot\left(\frac{\pi(n-j+1)}{n}\right),\\ a_{i+1,j+1}=a_{ij},\end{cases} \quad i,j=2,3,4,...,n,\ B^{(1)}=2\pi\left[a_{ij}\right], \quad (58)$$

$$\begin{cases}b_{11}=-\frac{n^2}{12}-\frac{1}{6},\\ b_{i,1}=\frac{(-1)^{i-1}}{2\sin^2\left(\frac{\pi(i-1)}{n}\right)},\\ b_{1,j}=\frac{(-1)^{n-j+1}}{2\sin^2\left(\frac{\pi(n-j+1)}{n}\right)},\\ b_{i+1,j+1}=b_{ij},\end{cases} \quad i,j=2,3,4,...,n,\ B^{(2)}=(2\pi)^2\left[b_{ij}\right]. \quad (59)$$

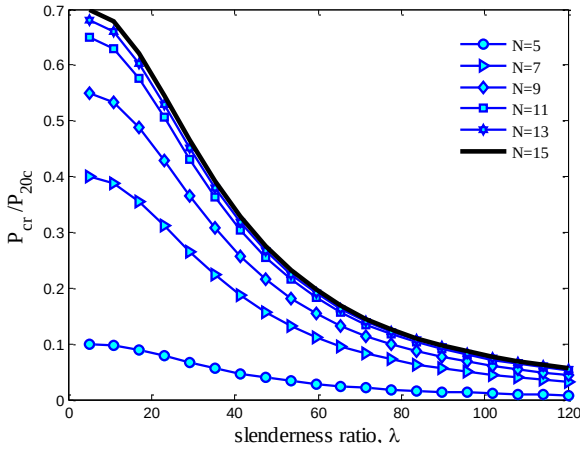

Fig. 2 Accuracy of DQM for critical buckling load

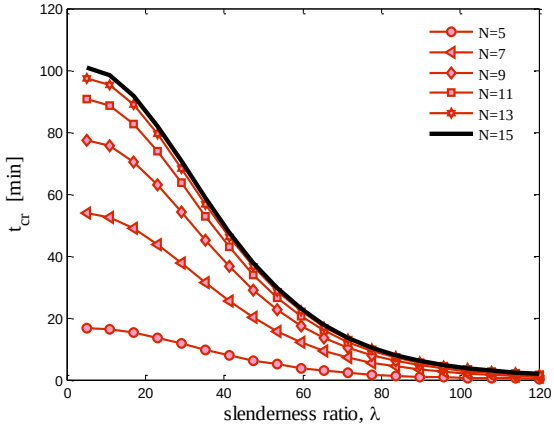

Fig. 3 Accuracy of DQM for critical buckling time

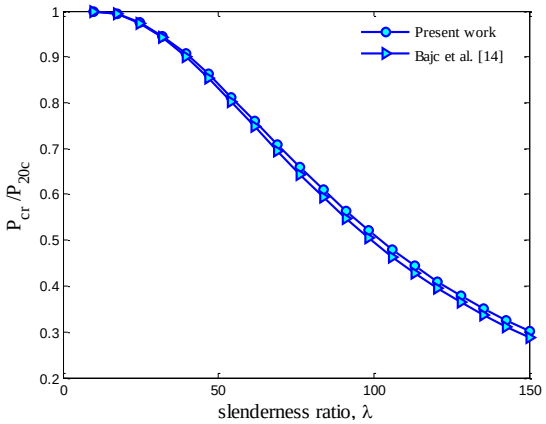

Fig. 4 Validation of critical buckling load

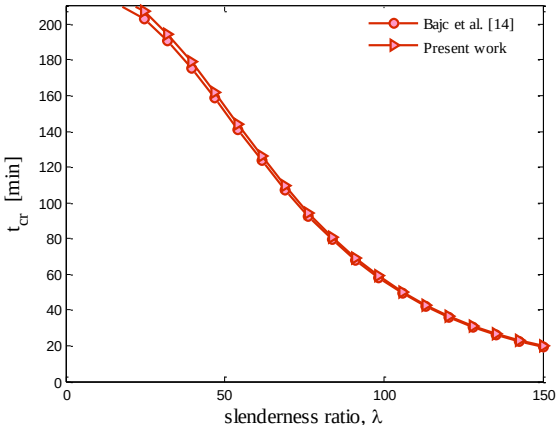

Fig. 5 Validation of critical buckling time

Using DQM, the governing equations can be expressed in matrix form as

$$\begin{Bmatrix} I \otimes \left(K_L + K_{NL}\right) + N_x^M \left[I \otimes K_g\right] + \\ \left[B^{(1)} \otimes C\right] + \\ \left[B^{(2)} \otimes M\right] \end{Bmatrix} \begin{Bmatrix} Y_b \\ Y_d \end{Bmatrix} = 0, \quad (60)$$

Where K_L is the linear stiffness matrix; K_{NL} is the nonlinear stiffness matrix; C is the coefficients of fist derivative to time, M is the coefficients of second derivative to time, K_g is geometric stiffness matrix; and $\otimes$ is the Kroniker product. Also, Y_b and Y_d represent boundary and domain points. Finally, based on an iterative method and eigenvalue problem,

• The critical buckling time t_{cr} can be obtained at the given constant load P.

• The critical buckling load P_{cr} at the selected time.

5. Numerical results

In this section, a concrete column with elastic modules of Em=20 GPa is considered which is reinforced with SiO_2nano-particles with elastic modules of Er=75 GPa. All of the properties related to fire are chosen from (Bajc *et al.* 2015). Based on DQM, the critical buckling load and critical buckling time of structure are calculated.

5.1 Accuracy of DQM

The effect of the grid point number in DQM on the critical buckling load and critical buckling time of the concrete column is demonstrated in Figs. 2 and 3, respectively. As can be seen, fast rate of convergence of the method are quite evident and it is found that 15 DQM grid points can yield accurate results. In addition, with increasing slenderness ratio (λ) of column, the critical buckling load and critical buckling time decrease due to reduction in stiffness of system.

5.2 Validation

In the absence of similar publications in the literature covering the same scope of the problem, one cannot directly validate the results found here. However, the present work could be partially validated based on a simplified analysis suggested by (Bajc *et al.* 2015) on buckling of the concrete column for which the nano-particles and elastic foundation (c_r=0, k_w=k_g=0) in this paper were ignored. The results are shown in Figs. 4 and 5 in which buckling load and critical buckling time versus slenderness ratio are plotted, respectively. As can be seen the two analyses agree well and show similar results.

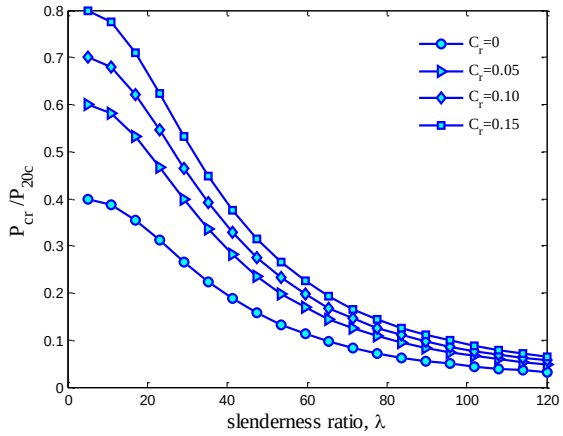

Fig. 6 The effect of SiO_2nano-particles volume percent on the critical buckling load

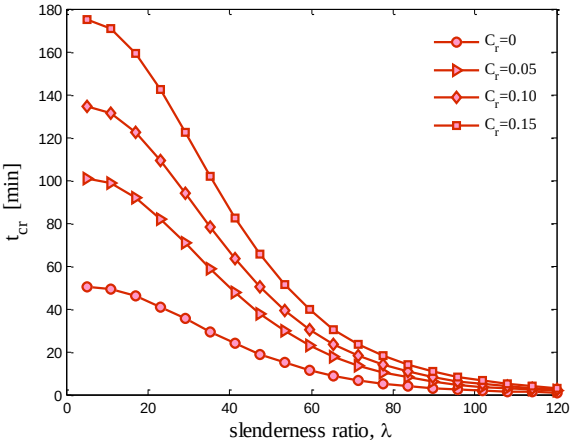

Fig. 7 The effect of SiO_2nano-particles volume percent on the critical buckling time

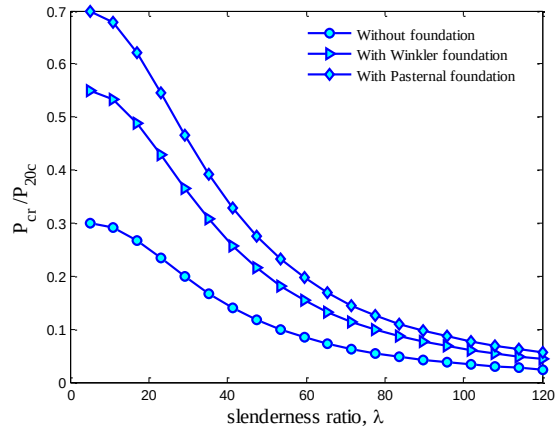

Fig. 8 The foundation effect on the critical buckling load

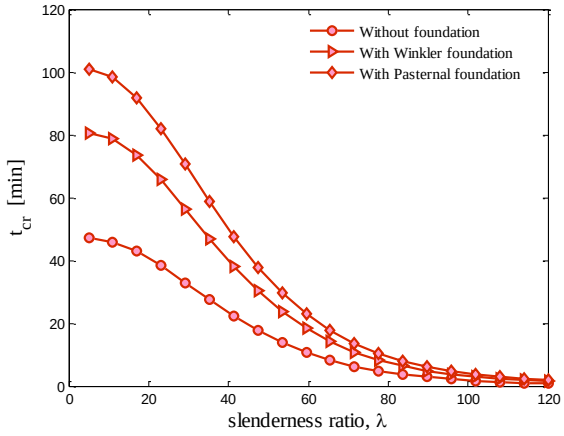

Fig. 9 The foundation effect on the critical buckling time

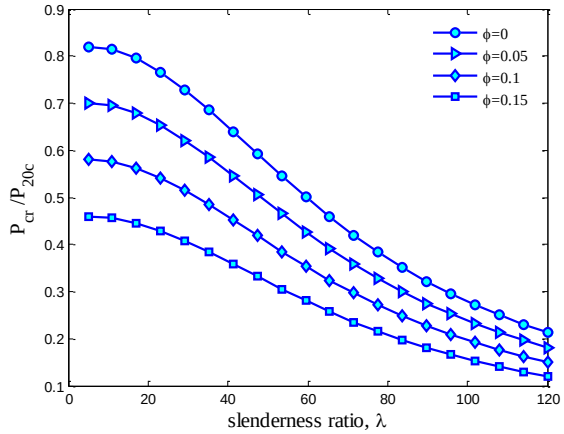

Fig. 10 The concrete porosity effect on the critical buckling load

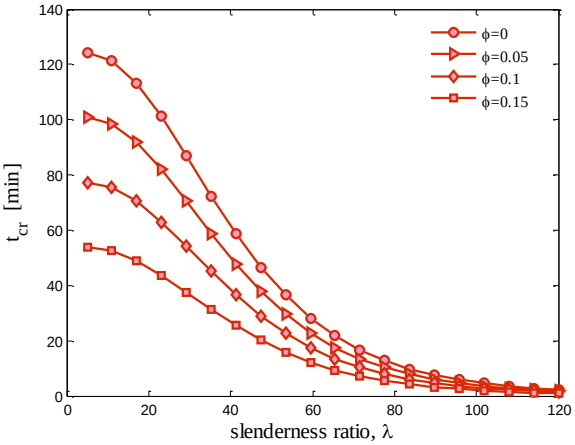

Fig. 11 The concrete porosity effect on the critical buckling time

5.3 The effect of different parameters

The effect of volume percent of SiO_2nano-particles on the time-dependent critical buckling load and critical buckling time of concrete column is illustrated in Figs. 6 and 7, respectively. It can be found that with increasing the volume percent of SiO_2nano-particles, the critical buckling load and critical buckling time increase. It is due to the fact that with increasing volume percent of SiO_2nano-particles, the stiffness of structure increases. Hence, the SiO_2nano-particles volume fraction is effective controlling parameters for critical buckling load and critical buckling time of the concrete column. In addition, the effect of volume percent of SiO_2nano-particles on the critical buckling load and critical buckling time load becomes prominent for short columns (λ<50).

Figs. 8 and 9 illustrate the influence of elastic medium on the critical buckling load and critical buckling time

along the slenderness ratio, respectively. Obviously, the foundation has a significant effect on the critical buckling load and critical buckling time of the column, since the critical buckling load and critical buckling time of the system in the case of without foundation are lower than other cases. It can be concluded that the critical buckling load and critical buckling time for Pasternak model (spring and shear constants) are higher than Winkler (spring constant) one. The above results are reasonable, since the Pasternak medium considers not only the normal stresses (i.e., Winkler foundation) but also the transverse shear deformation and continuity among the spring elements.

The effect of concrete porosity on the critical buckling load and critical buckling time of structure is showmen in Figs. 10 and 11, respectively. It can be found that increasing concrete porosity leads to higher critical buckling load and critical buckling time. It is reasonable since the stiffness of structure becomes lower with increasing concrete porosity.

6. Conclusions

The paper presents a new model for the SiO_2nano-particle reinforced concrete column exposed to fire theoretically for the first time. The Timoshenko beam model was used for mathematical modelling and the characteristics of the equivalent composite being determined using Mori-Tanaka rule. The governing mass conservation equations to describe heat and moisture transport in concrete containing free water, water vapor, and dry air in conjunction with the conversion of energy were considered. DQM and a direct iterative approach were employed to obtain the critical buckling load and critical buckling time. Results indicate that with increasing the volume percent of SiO_2nano-particle, the critical buckling load and critical buckling time increase. It was also worth to mention that increasing concrete porosity leads to higher critical buckling load and critical buckling time. Obviously, the foundation has a significant effect on the critical buckling load and critical buckling time of the column. In addition, the effect of volume percent of SiO_2nano-particles on the critical buckling load and critical buckling time load becomes prominent for short columns (λ<50). Finally, it is hoped that the results presented in this paper would be helpful for using nano-technology in concrete structures exposed to fire.

References

Bacinskas, D., Kaklauskas, G., Gribniak, V., Sung, W.P. and Shih, M.H. (2012), "Layer model for long-term deflection analysis of cracked reinforced concrete bending members", *Mech. Time Depend. Mater.*, **16**(2), 117-127.

Bajc, U., Saje, M., Planinc, I. and Bratina, S. (2015), "Semi-analytical buckling analysis of reinforced concrete columns exposed to fire", *Fire Saf. J.*, **71**, 110-122.

Bratina, S., Čas, B., Saje, M. and Planinc, I. (2005), "Numerical modelling of behaviour of reinforced concrete columns in fire and comparison with Eurocode 2", *J. Sol. Struct.*, **42**(21), 5715-5733.

Bratina, S., Saje, M. and Planinc, I. (2007), "The effects of different strain contributions on the response of RC beams in fire", *Eng. Struct.*, **29**(3), 418-430.

Brush, D.O. and Almroth, B.O. (1975), *Buckling of Bars, Plates and Shells*, McGraw-Hill, New York, U.S.A.

Capua, D.D. and Mari, A.R. (2007), "Nonlinear analysis of reinforced concrete cross-sections exposed to fire", *Fire Saf. J.*, **27**, 139-149.

Colin, T., Davie Chris, J. and Bic´anic, N. (2006), "Coupled heat and moisture transport in concrete at elevated temperatures-effects of capillary pressure and adsorbed water", *Numer. Heat Transf. Part A*, **49**(8), 733-763.

Franssen, J.M. and Dotreppe, J.C. (2003), "Fire tests and calculation methods for circular concrete columns", *Fire Technol.*, **39**(1), 89-97.

Ghorbanpour Arani, A., Kolahchi, R. and Zarei, M.S. (2015), "Visco-surface-nonlocal piezoelasticity effects on nonlinear dynamic stability of graphene sheets integrated with ZnO sensors and actuators using refined zigzag theory", *Compos. Struct.*, **132**, 506-526.

Hozjan, T., Planinc, I., Saje, M. and Srpčič, S. (2008), "Buckling of restrained steel columns due tofire conditions", *Steel Compos. Struct.*, **8**(2), 159-178.

Hozjan, T., Saje, M., Srpčič, S. and Planinc, I. (2011), "Fire analysis of steel-concrete composite beam with interlayer slip", *Steel Compos. Struct.*, **89**(1), 189-200.

Jafarian Arani, A. and Kolahchi, R. (2016), "Buckling analysis of embedded concrete columns armed with carbon nanotubes", *Comput. Concrete*, **17**(5), 567-578.

Kodur, V., Wang, T.C. and Cheng, F.P. (2004), "Predicting thefire resistance behavior of high strength concrete columns", *Cement Concrete Compos.*, **26**(2), 141-153.

Kolahchi, R., Rabani Bidgoli, M., Beygipoor, G. and Fakhar, M.H. (2015), "A nonlocal nonlinear analysis for buckling in embedded FG-SWCNT-reinforced microplates subjected to magnetic field", *J. Mech. Sci. Technol.*, **29**(9), 36695-3677.

Kolahchi, R., Safari, M. and Esmailpour, M. (2016), "Dynamic stability analysis of temperature-dependent functionally graded CNT-reinforced visco-plates resting on orthotropic elastomeric medium", *Compos. Struct.*, **150**, 255-265.

Mori, T. and Tanaka, K. (1973), "Average stress in matrix and average elastic energy of materials with misfitting inclusions", *Acta Metall. Mater.*, **21**(5), 571-574.

Rodrigues, J.P.C., Laím, L. and Correia, A.M. (2010), "Behaviour of fiber reinforced concrete columns in fire", *Compos. Struct.*, **92**(5), 1263-1268.

Safari Bilouei, B., Kolahchi, R. and Rabani Bidgoli, M. (2016), "Buckling of concrete columns retrofitted with nano-fiber reinforced polymer (NFRP)", *Comput. Concrete*, **18**(5), 1053-1063.

Shepherd, P. and Burgess, I. (2011), "On the buckling of axially restrained steel columns in fire", *Eng. Struct.*, **33**(10), 2832-2838.

Tan, K.H. and Yao, Y. (2003), "Fire resistance of four-face heated reinforced concrete columns", *J. Struct. Eng.*, **129**(9), 1220-1229.

Wang, W.H, Han, L.H., Tan, Q.H. and Tao, Z. (2016), *Tests on the Steel-Concrete Bond Strength in Steel Reinforced Concrete (SRC) Columns After Fire Exposure*, Fire The., In press.

Zamanian, M., Kolahchi, R. and Rabani Bidgoli, M. (2016), "Agglomeration effects on the buckling behaviour of embedded concrete columns reinforced with SiO_2nano-particles", *Wind Struct.*, **24**(1), 43-57.

CC

Appendix A

$$C_{TT} = \rho C + (\lambda_D + \lambda_E)\left(\varepsilon_D \frac{\partial \rho_L}{\partial t} + \rho_L \frac{\partial \varepsilon_D}{\partial t}\right) - \lambda_E\left(\varepsilon_{FW} \frac{\partial \rho_L}{\partial t} + \rho_L \frac{\partial \varepsilon_{FW}}{\partial t}\right), \tag{1}$$

$$C_{TP} = 0, \tag{2}$$

$$C_{TV} = -\lambda_E \rho_L \frac{\partial \varepsilon_{FW}}{\partial \bar{\rho}_V}, \tag{3}$$

$$C_{AT} = \bar{\rho}_A\left(\frac{\partial \phi}{\partial T} - \frac{\partial \varepsilon_{FW}}{\partial T}\right) - \frac{\varepsilon_G P_G}{R_A T^2}, \tag{4}$$

$$C_{AP} = \frac{\varepsilon_G}{R_A T}, \tag{5}$$

$$C_{AV} = -\frac{\varepsilon_G R_V}{R_A} - \bar{\rho}_A \frac{\partial \varepsilon_{FW}}{\partial \bar{\rho}_V}, \tag{6}$$

$$C_{MT} = \bar{\rho}_V \frac{\partial \phi}{\partial T} + (\varepsilon_{FW} - \varepsilon_D)\frac{\partial \rho_L}{\partial t} + (\rho_L - \bar{\rho}_V)\frac{\partial \varepsilon_{FW}}{\partial T} - \rho_L \frac{\partial \varepsilon_D}{\partial T}, \tag{7}$$

$$C_{MP} = 0, \tag{8}$$

$$C_{MV} = \varepsilon_G + (\rho_L - \bar{\rho}_V)\frac{\partial \varepsilon_{FW}}{\partial \bar{\rho}_V}, \tag{9}$$

$$K_{TT} = k, \tag{10}$$

$$K_{TP} = -\lambda_E \varepsilon_{FW} \rho_L \frac{\bar{K} K_L}{\mu_L}, \tag{11}$$

$$K_{TV} = 0, \tag{12}$$

$$K_{AT} = -\frac{\varepsilon_G D_{AV} \bar{\rho}_V P_G}{\bar{\rho}_G R_A T^2}, \tag{13}$$

$$K_{AP} = \frac{\bar{K} K_G}{\mu_G} \varepsilon_G \bar{\rho}_A + \frac{\varepsilon_G D_{AV} \bar{\rho}_V}{\bar{\rho}_G R_A T}, \tag{14}$$

$$K_{AV} = -\frac{\varepsilon_G D_{AV}}{\bar{\rho}_G}\left(\bar{\rho}_A + \frac{R_V \bar{\rho}_V}{R_A}\right), \tag{15}$$

$$K_{MT} = \frac{\varepsilon_G D_{AV} \bar{\rho}_V P_G}{\bar{\rho}_G R_A T^2}, \tag{16}$$

$$K_{MP} = \frac{\bar{K} K_G}{\mu_G} \varepsilon_G \bar{\rho}_V - \frac{\varepsilon_G D_{AV} \bar{\rho}_V}{\bar{\rho}_G R_A T} + \varepsilon_{FW} \rho_L \frac{\bar{K} K_L}{\mu_L}, \tag{17}$$

$$K_{MV} = \frac{\varepsilon_G D_{AV}}{\bar{\rho}_G}\left(\bar{\rho}_A + \frac{R_V \bar{\rho}_V}{R_A}\right), \tag{18}$$